

**Photoinduced EPR study of Sb<sup>2+</sup> ions in photorefractive Sn<sub>2</sub>P<sub>2</sub>S<sub>6</sub> crystals**A. T. Brant,<sup>1</sup> L. E. Halliburton,<sup>2,\*</sup> S. A. Basun,<sup>3,4</sup> A. A. Grabar,<sup>5</sup> S. G. Odoulov,<sup>6</sup> A. Shumelyuk,<sup>6</sup> N. C. Giles,<sup>1</sup> and D. R. Evans<sup>4</sup><sup>1</sup>*Department of Engineering Physics, Air Force Institute of Technology, Wright-Patterson Air Force Base, Ohio 45433, USA*<sup>2</sup>*Department of Physics, West Virginia University, Morgantown, West Virginia 26506, USA*<sup>3</sup>*Azimuth Corporation, 4134 Linden Avenue, Suite 300, Dayton, Ohio 45431, USA*<sup>4</sup>*Air Force Research Laboratory, Materials and Manufacturing Directorate, Wright-Patterson Air Force Base, Ohio 45433, USA*<sup>5</sup>*Institute of Solid State Physics and Chemistry, Uzhgorod National University, 88 000 Uzhgorod, Ukraine*<sup>6</sup>*Institute of Physics, National Academy of Sciences, 03 650 Kiev, Ukraine*

(Received 17 April 2012; published 10 October 2012)

Single crystals of Sn<sub>2</sub>P<sub>2</sub>S<sub>6</sub> are both ferroelectric and photorefractive. Antimony (Sb) ions are optically active in this material and play an important role in optimizing the photorefractive response. Electron paramagnetic resonance (EPR) is used to determine the site and charge states of the Sb ions in Sn<sub>2</sub>P<sub>2</sub>S<sub>6</sub> and to illustrate the photocharging behavior of these ions. In as-grown crystals, Sb<sup>3+</sup> ions substitute for Sn<sup>2+</sup> ions. A multiline EPR spectrum from Sb<sup>2+</sup> ions is observed after exposing a crystal at 30 K to either 633- or 442-nm laser light. These Sb<sup>2+</sup> ions are thermally stable at low temperature after the light is removed. They revert back to Sb<sup>3+</sup> ions when the crystal is warmed above 250 K for a few minutes. The EPR spectrum has  $S = 1/2$  and consists of well-resolved sets of hyperfine lines from <sup>121</sup>Sb and <sup>123</sup>Sb nuclei. Spin Hamiltonian parameters are obtained from the angular dependence of the spectrum (principal values are 1.810, 1.868, and 1.887 for the  $g$  matrix and 1404, 1687, and 1849 MHz for the <sup>121</sup>Sb hyperfine matrix). These parameters provide evidence that the wave function for the unpaired spin has significant  $p$ -like character and has overlap with neighboring ions.

DOI: [10.1103/PhysRevB.86.134109](https://doi.org/10.1103/PhysRevB.86.134109)

PACS number(s): 42.70.Nq, 77.84.-s, 76.30.Lh, 61.72.S-

**I. INTRODUCTION**

Single crystals of Sn<sub>2</sub>P<sub>2</sub>S<sub>6</sub> are an emerging unique and highly useful ferroelectric and photorefractive material.<sup>1-4</sup> Fast response times and high gain factors make this material well suited for photorefractive applications in the red and near-infrared regions of the spectrum.<sup>5-13</sup> Specific dopants, such as Sb, Te, and Bi, are known to significantly affect the wavelength response and the speed of the photorefractive effect in the Sn<sub>2</sub>P<sub>2</sub>S<sub>6</sub> crystals.<sup>14-19</sup> Doping with Sb ions introduces a near-edge optical absorption band that shifts the onset of transparency to longer wavelengths (from about 530 nm for an undoped crystal to near 650 nm when the Sb doping level is 2%).<sup>18</sup> A significant increase in the photorefractive gain factor for red light correlates with the presence of this Sb-related optical absorption band and its associated photoconductivity.<sup>15,18</sup> More recently, preilluminated Sb-doped crystals have been shown to contain secondary photorefractive centers that affect the dynamics of the beam coupling and cause transient beam fanning.<sup>20</sup> Until the present study, no candidates for these Sb-related secondary centers have been identified. The 0.33 eV activation energy reported<sup>20</sup> for the decay of these secondary centers is consistent with the thermal stability of the Sb<sup>2+</sup> ions described in the present investigation and thus establishes a direct link between our study and the photorefractive properties of Sb-doped Sn<sub>2</sub>P<sub>2</sub>S<sub>6</sub> crystals.

Despite their central role in the photorefractive mechanisms, little is known in general about point defects in Sn<sub>2</sub>P<sub>2</sub>S<sub>6</sub>. Intrinsic defects (vacancies, antisites, and interstitials) have not been extensively investigated in this material and extrinsic defects (impurities) have received only cursory attention. Major questions remain as to how individual point defects enhance or minimize the photorefractive effect in Sn<sub>2</sub>P<sub>2</sub>S<sub>6</sub>. The specific information needed about extrinsic defects includes site occupancy, possible charge states, thermal

stability of each charge state, and wavelength dependence of optically induced charge transfer processes. Similar detailed information is also needed about the intrinsic defects. With these goals in mind, we have initiated a research effort using photoinduced electron paramagnetic resonance (photo-EPR) to fundamentally characterize the photocharging of defects in Sn<sub>2</sub>P<sub>2</sub>S<sub>6</sub>. This experimental technique provides a sensitive method<sup>21</sup> to probe the structure and behavior of point defects in Sn<sub>2</sub>P<sub>2</sub>S<sub>6</sub> crystals, and it addresses basic questions about the identity and nature of the optically active defects in this important material. Preliminary EPR experiments on intrinsic defects in Sn<sub>2</sub>P<sub>2</sub>S<sub>6</sub> have been reported by Ruediger *et al.*,<sup>22,23</sup> and the EPR spectrum of Mn<sup>2+</sup> ions substituting for Sn<sup>2+</sup> ions in Sn<sub>2</sub>P<sub>2</sub>S<sub>6</sub> has been reported by Geifman *et al.*<sup>24</sup>

In the present paper, the photoinduced EPR technique is used to investigate Sb<sup>2+</sup> ions in single crystals of Sn<sub>2</sub>P<sub>2</sub>S<sub>6</sub> that have been intentionally doped with Sb. We find that Sb<sup>3+</sup> ( $5s^2$ ) ions substitute for Sn<sup>2+</sup> ( $5s^2$ ) ions in the as-grown crystals. Here, ionic notation is used to refer to the charge states of Sb and Sn. When the crystal is illuminated at 30 K with near-band-gap laser light, a portion of these Sb<sup>3+</sup> ions become photocharged with an electron and convert to the paramagnetic Sb<sup>2+</sup> ( $5s^25p^1$ ) charge state. Unique hyperfine patterns from the <sup>121</sup>Sb and <sup>123</sup>Sb nuclei provide direct evidence that the observed EPR signals are due to the Sb<sup>2+</sup> impurities. Data from a complete angular dependence study of the EPR spectrum are used to determine spin-Hamiltonian parameters for the Sb<sup>2+</sup> ions. Isochronal anneals at progressively higher temperatures provide information about the thermal stability of the photoinduced Sb<sup>2+</sup> ions. These ions return to the Sb<sup>3+</sup> charge state when the sample reaches approximately 250 K.

Only a few EPR studies of Sb ions are found in the literature. The most relevant are two papers that identify the singly ionized donor state of antimony (Sb) ions substituting for Ga

in bulk crystals of GaAs.<sup>25,26</sup> In semiconductor notation, this is the  $\text{Sb}_{\text{Ga}}^+$  heteroantisite defect. The EPR spectrum from this  $\text{Sb}_{\text{Ga}}^+$  donor is isotropic. Sets of hyperfine lines from both isotopes of Sb are resolved in these studies and the reported  $g$  value and  $^{121}\text{Sb}$  hyperfine parameter are 2.02 and 6600 MHz, respectively.

## II. EXPERIMENTAL DETAILS

The  $\text{Sn}_2\text{P}_2\text{S}_6$  crystals used in this investigation were grown by the vapor transport method at Uzhgorod National University in the Ukraine. Approximately 1% of Sb was added to the starting materials and iodine was used as the transport agent. The growth temperature was approximately 570 °C. EPR-sized samples with dimensions of  $0.5 \times 2.0 \times 2.5 \text{ mm}^3$  were cut from larger as-grown boules. Below the 64 °C phase transition, the  $\text{Sn}_2\text{P}_2\text{S}_6$  crystals are monoclinic with space group  $Pn$  and point group  $m$ . The lattice constants<sup>27,28</sup> are  $a = 9.378 \text{ \AA}$ ,  $b = 7.488 \text{ \AA}$ ,  $c = 6.513 \text{ \AA}$ , and  $\beta = 91.15^\circ$ . The second crystallographic setting is used where the  $b$  axis is perpendicular to the crystal's mirror plane. In the present study, the  $\text{Sn}_2\text{P}_2\text{S}_6$  crystals are considered to be orthorhombic when analyzing the EPR angular dependence data (i.e., the slight deviation from 90° between the  $a$  and  $c$  axes is ignored in the present analysis).

In general, the  $\text{Sn}_2\text{P}_2\text{S}_6$  crystal can be viewed as a collection of  $(\text{P}_2\text{S}_6)^{4-}$  anionic groups linked by  $\text{Sn}^{2+}$  ions. As illustrated schematically in Fig. 1, there are two inequivalent tin sites, two inequivalent phosphorus sites, and six inequivalent sulfur sites in the low-temperature phase. The focus in the present paper is on the  $\text{Sn}^{2+}$  sites. Above the phase change, the two  $\text{Sn}^{2+}$  sites are crystallographically equivalent. According to Scott *et al.*,<sup>28</sup> the two  $\text{Sn}^{2+}$  ions move by 0.32 and 0.22 Å, respectively, when a crystal is cooled (through the phase transition) from 110 °C to room temperature. Both of the  $\text{Sn}^{2+}$  displacements are primarily along the  $a$  direction and the Sn-Sn separation only changes from 8.727 to 8.690 Å when going from 110 °C to room temperature.<sup>28</sup> Each  $\text{Sn}^{2+}$  ion has eight sulfur neighbors in the low-temperature phase. These Sn-S separation distances

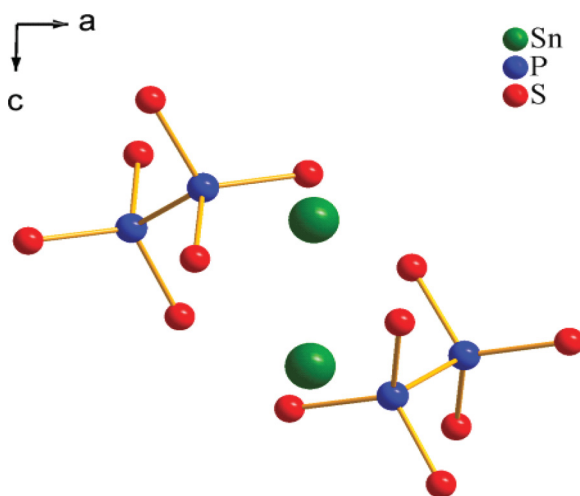


FIG. 1. (Color online) Schematic representation of the low-temperature monoclinic structure of  $\text{Sn}_2\text{P}_2\text{S}_6$  crystals. A projection on the  $b$  plane is shown.

vary from 2.876 to 3.516 Å for one  $\text{Sn}^{2+}$  site and from 2.781 to 3.455 Å for the other  $\text{Sn}^{2+}$  site.<sup>28</sup> The inequivalency of the two  $\text{Sn}^{2+}$  sites in the low-temperature phase is small and may not play a significant role in the present investigation.

The EPR spectra were taken with a Bruker EMX spectrometer operating near 9.5 GHz. An Oxford helium-gas-flow system was used to control the sample temperature and a proton NMR gaussmeter was used to measure the static magnetic fields. A Cr-doped MgO crystal was used to correct for the small difference in magnetic field between the sample and the probe tip of the gaussmeter (the isotropic  $g$  value for  $\text{MgO}:\text{Cr}^{3+}$  is 1.9800). The samples were illuminated at low temperature in the EPR microwave cavity with 442-nm light from a He-Cd laser or with 633-nm light from a He-Ne laser. The 442-nm light is above the band gap of the crystal and the 633-nm light is below the band gap.<sup>29</sup>

## III. EPR RESULTS

Figure 2 shows the EPR spectrum of  $\text{Sb}^{2+}$  ( $5s^25p^1$ ) ions in  $\text{Sn}_2\text{P}_2\text{S}_6$ . These data were taken at 30 K during exposure to 442-nm laser light. The magnetic field was parallel to the  $b$  axis of the crystal. Prior to illumination, no EPR signals were present. The spectrum in Fig. 2 contains a series of rather broad, yet well-resolved, hyperfine lines from the  $^{121}\text{Sb}$  and  $^{123}\text{Sb}$  nuclei (the separate sets are indicated by the upper stick diagrams). Widths of the individual lines vary from 2.0 to 3.0 mT. The  $^{121}\text{Sb}$  nuclei have  $I = 5/2$  and are 57.3% abundant, while the  $^{123}\text{Sb}$  nuclei have  $I = 7/2$  and are 42.7% abundant. There are six lines in the  $^{121}\text{Sb}$  set and eight lines in the  $^{123}\text{Sb}$  set, in agreement with the predicted  $2I + 1$  number of hyperfine lines for each isotope. Within each set, the separation of adjacent lines increases from low to high field, as expected when hyperfine parameters are large. The  $^{121}\text{Sb}$  nuclei have a

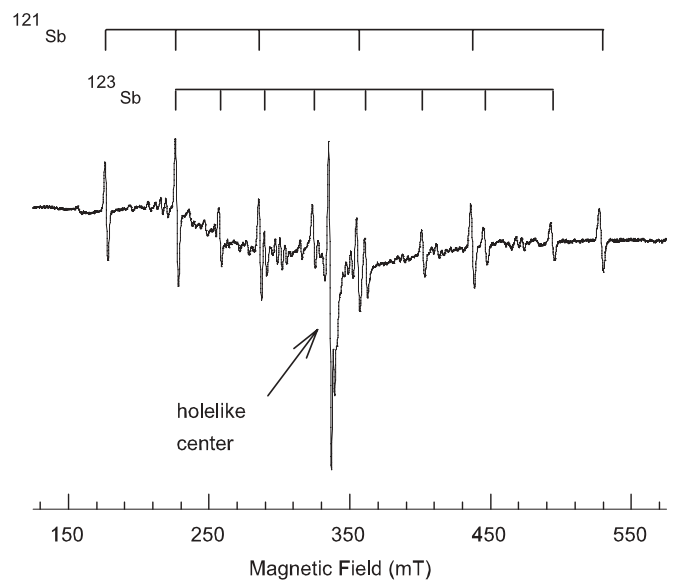


FIG. 2. EPR spectrum of  $\text{Sb}^{2+}$  ions in an  $\text{Sn}_2\text{P}_2\text{S}_6$  crystal. These data were taken at 30 K with the magnetic field along the  $b$  axis. The microwave frequency was 9.493 GHz. Stick diagrams illustrate the separate sets of  $^{121}\text{Sb}$  and  $^{123}\text{Sb}$  hyperfine lines. The more intense single line near the center of the spectrum is due to a holelike defect.

larger nuclear magnetic moment than the <sup>123</sup>Sb nuclei, thus accounting for the larger separations of the <sup>121</sup>Sb lines in the EPR spectrum. The maximum concentration of Sb<sup>2+</sup> ions produced at 30 K by the 442-nm laser was approximately  $2 \times 10^{18} \text{ cm}^{-3}$ . This estimate of concentration is based on a comparison of the EPR spectrum in Fig. 2 with a calibrated weak pitch EPR sample provided by Bruker. The same Sb<sup>2+</sup> EPR spectrum, about 20 times less intense, was observed when the crystal was cooled in the dark to 30 K and then exposed to 633-nm laser light.

An additional feature, one that is not Sb related, is present in Fig. 2. The single larger intensity EPR line near 335.67 mT exhibits behavior suggestive of a holelike center. This signal has very little angular dependence, remaining in a  $g$  value range of 2.005 to 2.026 for all orientations of magnetic field. After removing the laser light, this EPR signal is destroyed (i.e., becomes thermally unstable) when the sample temperature is raised above 70 K, thus indicating that the responsible defect has a relatively shallow ground-state energy level. This observation leads us to assign the holelike EPR signal in Fig. 2 to Sn<sup>3+</sup> ions. A Sn<sup>3+</sup> ( $5s^1$ ) ion is formed when a hole is localized on a Sn<sup>2+</sup> ( $5s^2$ ) ion in an otherwise unperturbed region of the lattice. This proposed model is an example of a small polaron.<sup>30–32</sup> For our microwave frequency of 9.5 GHz, the Sn<sup>3+</sup> ions are expected<sup>33,34</sup> to have a nearly isotropic EPR line at  $g \approx 2.0$  representing the nonmagnetic Sn nuclei (with  $I = 0$ ) that have no hyperfine interaction and a pair of less intense EPR lines near 480 mT representing the large hyperfine interactions with the <sup>117</sup>Sn and <sup>119</sup>Sn nuclei (each with  $I = 1/2$ ). The abundances of these two magnetic isotopes are 7.68% and 8.59%, respectively, while the combined abundance of the isotopes of Sn with  $I = 0$  is 83.39%. A detailed analysis of this EPR spectrum from Sn<sup>3+</sup> ions in Sn<sub>2</sub>P<sub>2</sub>S<sub>6</sub> will be provided in a later publication.

A complete angular dependence of the Sb<sup>2+</sup> EPR signals was acquired from a Sn<sub>2</sub>P<sub>2</sub>S<sub>6</sub> crystal. Sets of data were taken at increments of 15° in three planes (from  $a$  to  $b$ , from  $b$  to  $c$ , and from  $c$  to  $a$ ), as illustrated by the data points in Fig. 3. Data were also taken in the plane from  $c$  to the midpoint between  $a$  and  $b$ . Each EPR line in the Sb<sup>2+</sup> spectrum separates into two equally intense branches when the magnetic field is rotated from  $b$  toward  $a$  or  $c$  (i.e., in the  $a$  to  $b$  and  $b$  to  $c$  planes). This splitting is not resolved for a few of the lines in Fig. 3. The splitting into two branches shows that the Sb<sup>2+</sup> ions have two crystallographically equivalent, but magnetically inequivalent, orientations (i.e., sites) in this lattice. There is only one set of lines for each of the Sb<sup>2+</sup> isotopes when the magnetic field is along the  $a$ ,  $b$ , or  $c$  directions, thus demonstrating that the two orientations of the Sb<sup>2+</sup> ions are magnetically equivalent for these three directions. The EPR lines do not split into branches when the magnetic field is rotated from  $a$  to  $c$  (in the mirror plane) as the two orientations of the defect are magnetically equivalent for all angles in this plane.

The following spin Hamiltonian with  $S = 1/2$  was used to analyze the Sb<sup>2+</sup> EPR data.<sup>21</sup>

$$\mathbf{H} = \beta\mathbf{S} \cdot \mathbf{g} \cdot \mathbf{B} + \mathbf{I} \cdot \mathbf{A} \cdot \mathbf{S} - g_N\beta_N\mathbf{I} \cdot \mathbf{B} \quad (1)$$

The separate terms represent electron Zeeman, hyperfine, and nuclear Zeeman interactions, respectively. A nuclear

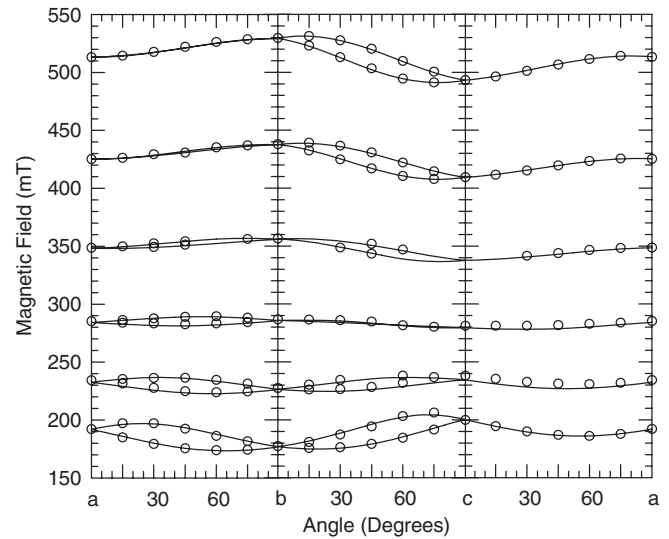


FIG. 3. EPR angular dependence of Sb<sup>2+</sup> ions in the  $a$  to  $b$ ,  $b$  to  $c$ , and  $c$  to  $a$  planes. Results for <sup>121</sup>Sb are shown. The solid curves were calculated using the  $\mathbf{g}$  and  $\mathbf{A}$  matrix parameters in Table I and a microwave frequency of 9.495 GHz. The discrete points are experimental results.

electric quadrupole term is not included in the spin-Hamiltonian since forbidden transitions are not observed in the Sb<sup>2+</sup> EPR spectrum. The  $\mathbf{g}$  and  $\mathbf{A}$  matrices in Eq. (1) are each described by six parameters (three principal values and three angles to specify the directions of the principal axes). These directions of principal axes play an important role in the present study. In particular, the two crystallographically equivalent, but magnetically inequivalent, orientations of the Sb<sup>2+</sup> ions referred to in the previous paragraph have the same principal values but different (symmetry-related) principal-axes directions. The observed separation of the Sb<sup>2+</sup> EPR lines into two branches when rotating in the  $a$  to  $b$  and the  $b$  to  $c$  planes (illustrated in Fig. 3) occurs because the  $\mathbf{g}$  and  $\mathbf{A}$  matrices do not have a principal axis along the  $b$  direction in the crystal (i.e., the direction perpendicular to the mirror plane).

We only determined values of the spin-Hamiltonian parameters for the <sup>121</sup>Sb nuclei, since there were fewer of these lines to identify in the spectrum and their intensities were larger. For the <sup>123</sup>Sb nuclei, it is expected that the  $\mathbf{g}$  matrix is the same and the principal values of the hyperfine  $\mathbf{A}$  matrix scale with the magnetic moments of the two isotopes. Final values of the <sup>121</sup>Sb parameters (both the  $\mathbf{g}$  and  $\mathbf{A}$  matrices) were obtained from a least-squares fitting procedure that involved exact diagonalizations of the  $12 \times 12$  spin-Hamiltonian matrix ( $S = 1/2$ ,  $I = 5/2$ ). The EPR spectra taken every 15° in the  $a$  to  $b$ ,  $b$  to  $c$ , and  $c$  to  $a$  planes provided the input data used to determine the “best-fit” values for the twelve parameters. Only the outer hyperfine lines (i.e., those at the lowest and highest magnetic fields) were included in the fitting. This gave, as input data, a total of 84 magnetic field values and their associated microwave frequencies from the three planes. As a final step, data obtained when the magnetic field was rotated from  $c$  to the midpoint between  $a$  and  $b$  was used to distinguish between two sets of parameters that fit the  $a$  to  $b$ ,  $b$  to  $c$ , and  $c$  to  $a$  data equally well. Table I contains the “best-fit”

TABLE I. Spin-Hamiltonian parameters for  $\text{Sb}^{2+}$  ions in  $\text{Sn}_2\text{P}_2\text{S}_6$  crystals. Values are given for the  $^{121}\text{Sb}$  isotope. Estimated error limits are  $\pm 0.005$  for the  $g$  values,  $\pm 20$  MHz for the  $A$  values, and  $\pm 3.0^\circ$  for the  $\theta$  and  $\phi$  angles.

	Principal Values	Principal-Axis Directions	
	$^{121}\text{Sb}$	$\theta$	$\phi$
	<b>g matrix</b>		
$g_1$	1.810	$68.7^\circ$	$218.6^\circ$
$g_2$	1.868	$49.6^\circ$	$109.2^\circ$
$g_3$	1.887	$48.0^\circ$	$329.2^\circ$
	<b>A hyperfine matrix</b>		
$A_1$	1404 MHz	$34.7^\circ$	$213.0^\circ$
$A_2$	1687 MHz	$121.9^\circ$	$187.3^\circ$
$A_3$	1849 MHz	$77.9^\circ$	$104.9^\circ$

values and estimates of error limits for the twelve parameters describing the  $\mathbf{g}$  and  $\mathbf{A}$  matrices. In Table I, the three Euler angles specifying the directions of the principal axes have been converted to  $(\theta, \phi)$  pairs. The polar angle  $\theta$  is defined relative to the  $c$  axis, and the azimuthal angle  $\phi$  is defined relative to the  $a$  axis with positive rotation from  $a$  toward  $b$  in the  $c$  plane. The directions listed in Table I refer to one of the two equivalent orientations of the principal-axis systems. The principal-axis directions for the other orientation are obtained by a reflection through the mirror plane of the crystal. Only the relative signs of the hyperfine principal values can be obtained from the experimental data. Positive signs have been chosen for the three principal values of the  $\mathbf{A}$  matrix in Table I because this matrix is highly isotropic and the nuclear magnetic moment of  $^{121}\text{Sb}$  is positive. Figure 3 shows the agreement between the measured and calculated angular dependence of the EPR spectrum in the three primary planes.

The  $\text{Sb}^{2+}$  EPR signals in Fig. 2 were not present before illumination. Once formed at 30 K, these signals are stable after the laser light is removed as long as the crystal remains at or near this temperature. The lines broaden beyond recognition at temperatures above 100 K because the spin-lattice relaxation time decreases as the temperature increases (the  $\text{Sb}^{2+}$  ions are not annihilated at 100 K since they reappear when the temperature is directly returned to 30 K from 100 K). An isochronal anneal experiment was performed to determine the thermal stability of the photoinduced  $\text{Sb}^{2+}$  ions. The sample was initially illuminated at 30 K. Then the light was removed and an EPR spectrum was taken at 30 K. Next, the sample temperature was increased to 75 K, held for 3 min at 75 K, and then returned to 30 K where the EPR spectrum was again taken. This incremental warming process was repeated at progressively higher temperatures (in steps of 25 K) with 3 min holding times. Following each step, the EPR spectrum was taken at the same 30 K monitoring temperature. These thermal decay results show that warming a previously illuminated crystal to 250 K for 3 min eliminates nearly all of the  $\text{Sb}^{2+}$  ions (they revert back to  $\text{Sb}^{3+}$  ions). The  $\text{Sb}^{2+}$  EPR signals are destroyed when the photoseparated charges (i.e., the electrons and holes) recombine and restore the crystal to its as-grown state. It is not known whether the thermally induced recombination process is initiated by the release of electrons from  $\text{Sb}^{2+}$  ions or the release of holes from the unidentified

holelike centers that become photocharged at the same time the  $\text{Sb}^{2+}$  ions are formed. After warming above 250 K for 3 min, the  $\text{Sb}^{2+}$  EPR signals in Fig. 2 reappear at low temperature only when the crystal is once again illuminated with laser light.

#### IV. DISCUSSION

Transient self-sensitizing of photorefraction has been shown to occur in crystals of  $\text{Sn}_2\text{P}_2\text{S}_6$  doped with Sb ions.<sup>20</sup> Specifically, preillumination of a doped sample with intense red light dramatically increases the two-beam coupling gain. This additional gain is, however, transient and disappears within several tens of seconds at room temperature after the pump light is removed. The model proposed in Ref. 20 attributes this unusual behavior of Sb-doped  $\text{Sn}_2\text{P}_2\text{S}_6$  to a light-induced increase of the effective trap density (which in turn reduces the charge screening effect). A light-induced variation of the effective trap density is possible only when at least two active centers are present in the crystal and each center can be recharged. A charge taken from a center of one type and transferred to a center of the other type results in a change in both their densities, i.e., there are changes in the density of donors and the density of traps. In a one-center model, the transfer of a charge from the donor to the trap does not result in a net change in the donor density and the trap density. The results described in Ref. 20 clearly show that an additional optically active center exists in Sb-doped  $\text{Sn}_2\text{P}_2\text{S}_6$  crystals and that its lifetime in the photoexcited charge state (about 14 s at room temperature) obeys the Arrhenius law with an activation energy  $\Delta E$  of approximately 0.33 eV.

It is reasonable to suppose that the secondary photorefractive center referred to in Ref. 20 is related to the presence of Sb because no other doped or nominally undoped  $\text{Sn}_2\text{P}_2\text{S}_6$  crystal shows similar nontrivial transient behavior in this time scale. The present paper provides results that allow us to conclude that the EPR-active  $\text{Sb}^{2+}$  ions are the secondary photorefractive centers responsible for the previously described transient gain enhancement. We have shown that the EPR spectrum of the  $\text{Sb}^{2+}$  ions appears in our samples only after illumination, that this charge state is stable at 30 K, and that these ions rapidly decay at temperatures near 250 K. The secondary centers observed in Ref. 20 are also light induced, and the temperature dependence of their lifetimes was measured in the temperature range from 257 to 320 K. According to the data in Fig. 4 of Ref. 20, the lifetime of the secondary centers is approximately 80 s for a temperature near 257 K. This is in agreement with our observations described in Sec. III. An extrapolation to 30 K of the lifetime of the secondary centers reported in Ref. 20 gives approximately  $0.5 \times 10^{50}$  s (i.e., these secondary centers should be absolutely stable at this lower temperature), and this is also in agreement with our thermal stability data for the  $\text{Sb}^{2+}$  EPR signals.

In addition to connecting the observed  $\text{Sb}^{2+}$  ions with the secondary photorefractive centers, an important contribution of the present paper is the complete characterization of the structural and spectroscopic properties of the Sb ions in  $\text{Sn}_2\text{P}_2\text{S}_6$  crystals. Our Sb-related EPR spectrum is assigned to  $\text{Sb}^{2+}$  ions replacing  $\text{Sn}^{2+}$  ions. The size (i.e., ionic radius) of the Sb ions is a much better match for the tin sites than the phosphorous sites. Also, if the Sb ions substitute for another

Group V ion such as phosphorus, they would not easily change their charge state, in contrast to the observed results. Although there are two crystallographically inequivalent  $\text{Sn}^{2+}$  sites in the low-temperature monoclinic  $\text{Sn}_2\text{P}_2\text{S}_6$  lattice (see Sec. II), only one  $\text{Sb}^{2+}$  EPR spectrum is observed. There are two plausible explanations for this result: (1) only one of the two  $\text{Sn}^{2+}$  sites is occupied by  $\text{Sb}^{3+}$  ions during growth or (2) both of the  $\text{Sn}^{2+}$  sites are occupied by  $\text{Sb}^{3+}$  ions during growth, but only those  $\text{Sb}^{3+}$  ions on one of the two sites are converted to  $\text{Sb}^{2+}$  ions by the laser light.

In the as-grown crystals, the nonparamagnetic  $\text{Sb}^{3+}$  ions have the same electron configuration ( $5s^2$ ) as the  $\text{Sn}^{2+}$  ions they replace. Paramagnetic  $\text{Sb}^{2+}$  ions are then formed by photocharging during illumination with laser light at low temperature. Although covalency effects are expected, these  $\text{Sb}^{2+}$  ions are best described as having a  $5s^25p^1$  configuration. This electron configuration suggests that the EPR spectrum of  $\text{Sb}^{2+}$  should reflect a significant  $p$ -like contribution. Both the  $\mathbf{g}$  and the  $\mathbf{A}$  matrices in Table I support this expectation. All of the principal values of the  $\mathbf{g}$  matrix have large shifts from the free-electron value of 2.0023, which indicates a large Sb spin-orbit interaction (and thus a significant non- $s$ -like contribution to the wave function). In addition, the principal values of the  $\mathbf{g}$  matrix suggest an axial character with the unique direction associated with the 1.810 principal value. The  $\mathbf{A}$  hyperfine matrix has significant anisotropy and this also implies a  $p$  orbital contribution. The isotropic (Fermi contact) part of the hyperfine matrix in Table I is  $a = 1646$  MHz where  $a = (A_1 + A_2 + A_3)/3$ . Morton and Preston<sup>35</sup> predict that an antimony  $5s$  electron has  $a = 35100$  MHz. These values indicate a 4.7% contribution to the  $\text{Sb}^{2+}$  EPR spectrum from the  $5s$  orbital. The anisotropic part of the hyperfine matrix in Table I is approximately  $b = 148$  MHz (i.e., one-third of the difference between  $A_1$  and  $A_3$ ), while Morton and Preston<sup>35</sup> predict that an antimony  $5p$  electron has  $b = 629$  MHz (2/5 of 1572 MHz). This suggests that the contribution to the  $\text{Sb}^{2+}$  EPR spectrum from the  $5p$  orbital may approach 23.5%. These  $s$  and  $p$  results place less than half of the unpaired spin on the Sb ion and imply that much of the spin must be distributed over one or more neighboring ions. Since the  $\text{Sb}^{2+}$  ions substituting for  $\text{Sn}^{2+}$  ions in  $\text{Sn}_2\text{P}_2\text{S}_6$  crystals can be viewed as a relatively shallow neutral donor ( $D^0$ ), this degree of delocalized behavior is reasonable.

The holelike centers that provide charge compensation for the electrons localized as  $\text{Sb}^{2+}$  ions are not identified in the present study. We note that the hole center observed in Fig. 2 (assigned to  $\text{Sn}^{3+}$  ions) is not a candidate for these compensating defects because its EPR signal decays (i.e., become thermally unstable) near 70 K, which is well below 250 K where the  $\text{Sb}^{2+}$  ions thermally decay. A likely candidate for the necessary compensating defects is a hole localized on a sulfur ion adjacent to a  $\text{Sn}^{2+}$  vacancy.<sup>36</sup> The  $\text{Sn}^{2+}$  vacancies are expected to be present in as-grown Sb-doped crystals because they would provide charge compensation for the substitutional  $\text{Sb}^{3+}$  ions. (One  $\text{Sn}^{2+}$  vacancy compensates two  $\text{Sb}^{3+}$  ions in an as-grown crystal.) These proposed sulfur-based vacancy-associated holelike centers would have small, but positive,  $g$  shifts and little or no observable hyperfine contributions. Motional effects or extreme spin-lattice relaxation times may make it challenging to observe their EPR spectrum in  $\text{Sn}_2\text{P}_2\text{S}_6$

crystals. Similar paramagnetic sulfur-related hole centers stabilized by an adjacent cation vacancy have been reported in the literature for other materials.<sup>37,38</sup>

## V. SUMMARY

Single crystals of  $\text{Sn}_2\text{P}_2\text{S}_6$  are doped with antimony (Sb) ions and then characterized using photo-EPR. The as-grown crystals contain  $\text{Sb}^{3+}$  ions substituting for  $\text{Sn}^{2+}$  ions. These  $\text{Sb}^{3+}$  ions convert to paramagnetic  $\text{Sb}^{2+}$  ions when they are photocharged with an electron during exposure at low temperature to 442- or 633-nm laser light. A thermal warming study shows that the photoinduced  $\text{Sb}^{2+}$  electron centers decay when the crystal is held near 250 K for a few minutes (i.e., they are not stable at room temperature). The EPR spectrum of the  $\text{Sb}^{2+}$  ions (with the  $5s^25p^1$  configuration) is dominated by well-resolved hyperfine lines from the  $^{121}\text{Sb}$  and  $^{123}\text{Sb}$  nuclei. A complete set of angular-dependence data taken in the  $a$  to  $b$ ,  $b$  to  $c$ , and  $c$  to  $a$  planes is used to obtain values for the  $g$  and  $^{121}\text{Sb}$  hyperfine matrices. Large shifts of the principal values of the  $\mathbf{g}$  matrix from the free-spin value of 2.0023 and significant anisotropy in the hyperfine patterns both indicate a significant  $5p$  contribution to the wave function of the unpaired electron.

These optically active Sb impurities are of considerable interest because of their major effect on the photorefractive response of the material, i.e., they act as secondary photorefractive centers<sup>20</sup> and transiently enhance the gain factor in the red portion of the spectrum.<sup>15,18</sup> The EPR-observed photocharging of a significant amount of  $\text{Sb}^{3+}$  to  $\text{Sb}^{2+}$  (on the order of  $10^{18}$   $\text{cm}^{-3}$ ) is caused when electrons are transferred from intrinsic photorefractive centers in the  $\text{Sn}_2\text{P}_2\text{S}_6$  crystals. After being formed, the photogenerated  $\text{Sb}^{2+}$  ions act as hole traps. (Holes have been shown to be the primary mobile charge species responsible for the photorefractive effect in  $\text{Sn}_2\text{P}_2\text{S}_6$ .<sup>39</sup>) These photoinduced effects alter the “effective trap density” and, in turn, modify the photorefractive gain in Sb-doped  $\text{Sn}_2\text{P}_2\text{S}_6$  crystals.<sup>13</sup> The correlated photoinduced changes in the concentrations of the  $\text{Sb}^{2+}$  ions and the intrinsic photorefractive centers that trap holes are short lived at room temperature. A decay time of approximately 14 s, reported in Ref. 20 and verified in the present study, makes the photoinduced changes in trap densities depend strongly on the intensity of the light that converts the  $\text{Sb}^{3+}$  ions to  $\text{Sb}^{2+}$  ions. This explains both the time dependent and power dependent character of the photorefractive gain observed in Sb-doped  $\text{Sn}_2\text{P}_2\text{S}_6$  crystals after pre-exposure to a strong pump beam and also explains the observed enhanced beam coupling under strong steady-state pumping.<sup>15,18,20</sup>

## ACKNOWLEDGMENTS

This research was supported at West Virginia University by Grant No. DMR-0804352 from the National Science Foundation and in the Ukraine by the European Office of Research and Development via the Science and Technology Center (Project P438 at Uzhgorod National University and Project P335 at the Institute of Physics in Kiev). The views expressed in this paper are those of the authors and do not necessarily reflect the official policy or position of the Air Force, the Department of Defense, or the United States Government.

\*Corresponding author: larry.halliburton@mail.wvu.edu

- <sup>1</sup>K. Z. Rushchanskii, Y. M. Vysochanskii, and D. Strauch, *Phys. Rev. Lett.* **99**, 207601 (2007).
- <sup>2</sup>J. Hlinka, R. Currat, M. de Boissieu, F. Livet, and Y. M. Vysochanskii, *Phys. Rev. B* **71**, 052102 (2005).
- <sup>3</sup>J. Hlinka, I. Gregora, and V. Vorliceck, *Phys. Rev. B* **65**, 064308 (2002).
- <sup>4</sup>J. Grigas, E. Talik, V. Lazauskas, Yu. M. Vysochanskii, R. Yevych, M. Adamiec, and V. Nelkinas, *Ferroelectrics* **378**, 70 (2009).
- <sup>5</sup>S. G. Odoulov, A. N. Shumelyuk, U. Hellwig, R. A. Rupp, and A. A. Grabar, *Opt. Lett.* **21**, 752 (1996).
- <sup>6</sup>S. G. Odoulov, A. N. Shumelyuk, U. Hellwig, R. A. Rupp, A. A. Grabar, and I. M. Stoyka, *J. Opt. Soc. Am. B* **13**, 2352 (1996).
- <sup>7</sup>S. G. Odoulov, A. N. Shumelyuk, G. A. Brost, and K. M. Magde, *Appl. Phys. Lett.* **69**, 3665 (1996).
- <sup>8</sup>M. Jazbinsek, G. Montemezzani, P. Gunter, A. A. Grabar, I. M. Stoika, and Y. M. Vysochanskii, *J. Opt. Soc. Am. B* **20**, 1241 (2003).
- <sup>9</sup>M. Jazbinsek, D. Haertle, G. Montemezzani, P. Gunter, A. A. Grabar, I. M. Stoika, and Y. M. Vysochanskii, *J. Opt. Soc. Am. B* **22**, 2459 (2005).
- <sup>10</sup>R. Mosimann, D. Haertle, M. Jazbinsek, G. Montemezzani, and P. Gunter, *J. Opt. Soc. Am. B* **23**, 1620 (2006).
- <sup>11</sup>B. Sturman, P. Mathey, H. R. Jauslin, S. Odoulov, and A. Shumelyuk, *J. Opt. Soc. Am. B* **24**, 1303 (2007).
- <sup>12</sup>A. Shumelyuk, A. Hryhorashchuk, S. Odoulov, and D. R. Evans, *Opt. Lett.* **32**, 1959 (2007).
- <sup>13</sup>A. Shumelyuk, S. Odoulov, G. Cook, and D. R. Evans, *Opt. Lett.* **34**, 2126 (2009).
- <sup>14</sup>T. Bach, M. Jazbinsek, P. Gunter, A. A. Grabar, I. M. Stoika, and Y. M. Vysochanskii, *Opt. Express* **13**, 9890 (2005).
- <sup>15</sup>T. Bach, M. Jazbinsek, G. Montemezzani, P. Gunter, A. A. Grabar, and Y. M. Vysochanskii, *J. Opt. Soc. Am. B* **24**, 1535 (2007).
- <sup>16</sup>R. Mosimann, P. Marty, T. Bach, F. Juvalta, M. Jazbinsek, P. Gunter, and A. A. Grabar, *Opt. Lett.* **32**, 3230 (2007).
- <sup>17</sup>I. V. Kedyk, P. Mathey, G. Gadret, O. Bidault, A. A. Grabar, I. M. Stoika, and Y. M. Vysochanskii, *J. Opt. Soc. Am. B* **25**, 180 (2008).
- <sup>18</sup>I. V. Kedyk, P. Mathey, G. Gadret, A. A. Grabar, K. V. Fedyo, I. M. Stoika, I. P. Prits, and Y. M. Vysochanskii, *Appl. Phys. B* **92**, 549 (2008).
- <sup>19</sup>Y. Kojima, A. Okamoto, A. A. Grabar, M. Takabayashi, and K. Shimayabu, *Ferroelectrics* **378**, 121 (2009).
- <sup>20</sup>D. R. Evans, A. Shumelyuk, G. Cook, and S. Odoulov, *Opt. Lett.* **36**, 454 (2011).
- <sup>21</sup>J.-M. Spaeth and H. Overhof, *Point Defects in Semiconductors and Insulators: Determination of Atomic and Electronic Structure from Paramagnetic Hyperfine Interactions*, Springer Series of Materials Science, Vol. 51 (Springer, Berlin, 2003).
- <sup>22</sup>A. Ruediger, O. Schirmer, S. Odoulov, A. Shumelyuk, and A. Grabar, *Opt. Mater.* **18**, 123 (2001).
- <sup>23</sup>Andreas Rüdiger, *Light Induced Charge Transfer Processes and Pyroelectric Luminescence in Sn<sub>2</sub>P<sub>2</sub>S<sub>6</sub>*, Ph.D. dissertation, University of Osnabrück, Osnabrück, Germany, 2001.
- <sup>24</sup>I. N. Geifman, I. V. Kozlova, U. M. Vysochanski, V. Ya. Kofman, and O. A. Mikailo, *Appl. Magn. Reson.* **2**, 435 (1991).
- <sup>25</sup>M. Baeumler, J. Schneider, U. Kaufmann, W. C. Mitchel, and P. W. Yu, *Phys. Rev. B* **39**, 6253 (1989).
- <sup>26</sup>P. Omling, D. M. Hofmann, M. Kunzer, M. Baeumler, and U. Kaufmann, *Phys. Rev. B* **45**, 3349 (1992).
- <sup>27</sup>G. Dittmar and H. Schäfer, *Z. Naturforsch.* **29b**, 312 (1974).
- <sup>28</sup>B. Scott, M. Pressprich, R. D. Willet, and D. A. Cleary, *J. Solid State Chem.* **96**, 294 (1992).
- <sup>29</sup>R. V. Gamernyk, Yu. P. Gnatenko, P. M. Bukivskij, P. A. Skubenko, and V. Yu. Slivka, *J. Phys.: Condens. Matter* **18**, 5323 (2006).
- <sup>30</sup>A. L. Shluger and A. M. Stoneham, *J. Phys.: Condens. Matter* **5**, 3049 (1993).
- <sup>31</sup>O. F. Schirmer, *J. Phys.: Condens. Matter* **18**, R667 (2006).
- <sup>32</sup>O. F. Schirmer, M. Imlau, C. Merschjann, and B. Schoke, *J. Phys.: Condens. Matter* **21**, 123201 (2009).
- <sup>33</sup>K. Sugibuchi, *Phys. Rev.* **153**, 404 (1967).
- <sup>34</sup>S. V. Nistor, D. Schoemaker, and I. Ursu, *Phys. Status Solidi B* **185**, 9 (1994).
- <sup>35</sup>J. R. Morton and K. F. Preston, *J. Magn. Reson. (1969–1992)* **30**, 577 (1978).
- <sup>36</sup>Yu. Vysochanskii, K. Glukhov, K. Fedyo, and R. Yevych, *Ferroelectrics* **414**, 30 (2011).
- <sup>37</sup>V. Seeman, M. Danilkin, E. Pärnoja, L. Pung, A. Ots, and A. Lorentz, *Solid State Commun.* **113**, 171 (2000).
- <sup>38</sup>V. Seeman, M. Danilkin, M. Must, A. Ots, E. Pärnoja, L. Pung, and K. Tarkpea, *Phys. Status Solidi B* **243**, 1978 (2006).
- <sup>39</sup>I. Seres, S. Stepanov, S. Mansurova, and A. Grabar, *J. Opt. Soc. Am. B* **17**, 1986 (2000).